
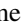


Interfacial characteristics, Schottky contact, and optical performance of a graphene/Ga₂SSe van der Waals heterostructure: Strain engineering and electric field tunability

Hong T. T. Nguyen ^{1,2,*}, Mohammed M. Obeid ³, Asadollah Bafekry^{4,11}, M. Idrees,⁵ Tuan V. Vu,^{1,2} Huynh V. Phuc ⁶,
 Nguyen N. Hieu,^{7,8} Le T. Hoa,^{7,8} Bin Amin ⁹, and Chuong V. Nguyen ^{10,†}

¹*Division of Computational Physics, Institute for Computational Science, Ton Duc Thang University, Ho Chi Minh City, Vietnam*

²*Faculty of Electrical & Electronics Engineering, Ton Duc Thang University, Ho Chi Minh City, Vietnam*

³*Department of Ceramics, College of Materials Engineering, University of Babylon, Hilla 51002, Iraq*

⁴*Department of Physics, University of Antwerp, Groenenborgerlaan 171, B-2020 Antwerp, Belgium*

⁵*Department of Physics, Hazara University, Mansehra 21300, Pakistan*

⁶*Division of Theoretical Physics, Dong Thap University, Dong Thap 93000, Vietnam*

⁷*Institute of Research and Development, Duy Tan University, Da Nang 550000, Vietnam*

⁸*Faculty of Natural Sciences, Duy Tan University, Da Nang 550000, Vietnam*

⁹*Department of Physics, Abbottabad University of Science and Technology, Abbottabad 22010, Pakistan*

¹⁰*Department of Materials Science and Engineering, Le Quy Don Technical University, Ha Noi 100000, Vietnam*

¹¹*Department of Physics, University of Guilan, 41335-1914 Rasht, Iran*



(Received 14 June 2020; revised 23 July 2020; accepted 27 July 2020; published 7 August 2020)

Two-dimensional graphene-based van der Waals heterostructures have received considerable interest because of their intriguing characteristics compared with the constituent single-layer two-dimensional materials. Here, we investigate the interfacial characteristics, Schottky contact, and optical performance of graphene/Ga₂SSe van der Waals (vdW) heterostructure using first-principles calculations. The effects of stacking patterns, electric gating, and interlayer coupling on the interfacial properties of graphene/Ga₂SSe heterostructures are also examined. Our results demonstrate that the Dirac cone of graphene is well preserved at the Γ point in all stacking patterns due to the weak vdW interactions, which keep the heterostructures feasible such that they can be obtained in further experiments. Moreover, depending on the stacking patterns, a small band gap of about 13–17 meV opens in graphene and has a high carrier mobility, indicating that the graphene/Ga₂SSe heterostructures are potential candidates for future high-speed nanoelectronic applications. In the ground state, the graphene/Ga₂SSe heterostructures form an *n*-type Schottky contact. The transformation from an *n*-type to a *p*-type Schottky contact or to an Ohmic contact can be forced by electric gating or by varying the interlayer coupling. Our findings could provide physical guidance for designing controllable Schottky nanodevices with high electronic and optical performances.

DOI: [10.1103/PhysRevB.102.075414](https://doi.org/10.1103/PhysRevB.102.075414)

I. INTRODUCTION

Following the successful exfoliation of single-layer graphene [1] in the past decade, many novel two-dimensional materials (2DMs) with unusual physicochemical properties have been discovered and investigated both theoretically and experimentally with an eye to nanoelectronics, optoelectronics, and valleytronics. Owing to the intriguing properties, including high mobility [2] and quantum Hall conductance [3], graphene is promising in a wide range of practical applications, such as field-effect transistors (FETs) [4] and transparent conductors [5]. Nevertheless, wider applications of graphene in various fields have been limited due to the lack of an electronic band gap. Different from graphene, most 2DMs possess a semiconducting nature with a sizable band gap of about 2–3 eV [6–8], which is suitable for various applications, such as photodetectors [9,10], FETs [11,12],

and so forth. To date, a lot of novel 2DMs, such as transition metal dichalcogenides (TMDCs) [13–15], phosphorene analogs [16–18], and graphitic carbon nitride [19,20], have been discovered. However, similar to graphene, these 2DMs also exhibit some drawbacks that may limit their potential applications. For instance, the wide band gap (~ 6 eV) [21] of hexagonal boron nitride hinders its applications in photocatalysis. Furthermore, the low carrier mobility ($200 \text{ cm}^2/\text{V s}$) [22] at room temperature of the MoS₂ TMDC has limited its applications in nanoelectronics. Therefore, the search for common strategies that can overcome these limitations in novel 2DMs is an important challenge in the scientific community along with the search for novel 2DMs.

Recently, vertical heterostructures (VHTs) combining two or more different 2DMs have proved to be a powerful strategy that not only combines most advantages of 2DMs but also introduces unusual physical properties, enhanced optical performance, and novel phenomena [23–28]. Many theoretical predictions and experimental preparations have confirmed that VHTs are great candidates for high-performance applications [26,29–31]. For instance, Zhou

*nguyenthithanhong@tdtu.edu.vn

†Corresponding author: chuongnguyen11@gmail.com

et al. [29] showed that the SnSe₂/MoS₂ VHT possesses a high responsivity of 9.1×10^3 A/W, suitable for high-efficiency photodetectors. Among 2DM-based VHTs, graphene-based VHTs have received much consideration because of the intriguing properties of perfect graphene. Currently, many VHTs based on graphene and other 2DMs have been proposed, such as graphene/MoS₂ [32–34], graphene/phosphorene [35,36], graphene/MXene [37–39], graphene/SnSe(S)₂ [40], graphene/GeC [41–43], graphene/GaS(Se) [44–47], and so on. All these graphene-based VHTs not only preserve all the key properties of graphene and 2DM monolayers but also show many interesting new properties and phenomena. For instance, Li *et al.* [37] reported that the formation of graphene/MXene VHTs causes a shift of the graphene Dirac point to higher or lower binding energy and results in an opening band gap in graphene. Earlier, Ben Aziza *et al.* [44] experimentally confirmed that the formation of the graphene/GaSe VHT leads to a shift in the graphene Dirac point to lower binding energy. Ning *et al.* [48] theoretically predicted that the optical absorption of the graphene/InAs VHT is significantly enhanced compared to those of the constituent monolayers.

More recently, a new kind of 2DM, namely, Janus 2DMs, has been discovered and successfully synthesized [49,50]. Following these successful productions in experiments of a Janus MoSSe monolayer [49,50], various types of Janus 2DMs have been theoretically predicted, such as Janus TMDCs [51,52], Janus M_2XY ($M = \text{Ga, In}$; $X/Y = \text{S, Se, Te}$) [53], and Janus MoSO [54,55]. Different from conventional 2DMs, Janus 2DMs possess large Rashba spin splitting and strong in-plane piezoelectricity, rendering them promising candidates for future applications in spintronics and valleytronics.

On the other hand, many VHTs from stacking graphene on Janus 2DMs have been proposed [56–60]. The contact between graphene and Janus 2DMs is a candidate for novel designs of 2D metal/semiconductor heterojunctions, forming either Schottky or Ohmic contacts. Cavalcante *et al.* [57] reported that stacking layers between the Janus MoSSe layers and graphene are a powerful strategy to select plasmonic frequencies of graphene. Cao *et al.* [60] demonstrated that the contact types forming in the graphene/PtSSe VHT can be adjusted by various methods, such as strain engineering, electric field, and the number of stacking layers. Although the graphene/GaS and graphene/GaSe VHTs have been studied both theoretically and experimentally [44–47], the interfacial characteristics and contact types in the graphene/Ga₂SSe VHT have not yet been investigated thoroughly. In addition, there are some common methods that can be used for the synthesis of 2D materials and their heterostructures, including mechanical or liquid-phase exfoliation and chemical vapor deposition (CVD) or epitaxial growth. For example, the graphene/MoS₂ heterostructure has been synthesized by a transfer method [24]. The GaSe/graphene heterostructure has been synthesized in experiment by molecular beam epitaxy [44] and the CVD technique [61]. Thus, we believe that the graphene/Ga₂SSe heterostructure can also be synthesized in experiments by a transfer method, molecular beam epitaxy, or the CVD method. Therefore, in this work, we investigate

the interfacial characteristics, Schottky contact, and optical performance of graphene/Ga₂SSe van der Waals heterostructure using first-principles calculations. The effects of stacking patterns, electric gating, and interlayer coupling on the interfacial properties of graphene/Ga₂SSe heterostructures are also examined. Our work is organized as follows: Details of the computational methodology are provided in Sec. II. The band alignment and contact types of the graphene/Ga₂SSe heterostructure along with the effects of strain and electric field are discussed and presented in Sec. III.

II. COMPUTATIONAL DETAILS

All the calculated results were obtained by means of density functional theory (DFT) and were simulated in the QUANTUM ESPRESSO package [62,63]. The exchange-correlation functional was approximated by the generalized gradient approximation [64], which was proposed by Perdew, Burke, and Ernzerhof [65]. The interactions between electrons and ions in all systems are carried out using the projector augmented-wave approach [66]. The Kohn-Sham orbitals were taken into account using a plane wave basis set. To correctly describe the weak forces in layered materials, the DFT-D3 method with a semiempirical dispersion potential is used for all calculations. The cutoff energy is set to be 510 eV, and a $(9 \times 9 \times 1)$ k -point grid of the first Brillouin zone (BZ) was performed for a Monkhorst-Pack mesh. In order to break unphysical interactions between periodic images of the system, a large vacuum of 30 Å was applied along the z direction. The convergence criterion of energy in the self-consistency process was set to be 10^{-6} eV. All the geometric optimization processes were obtained when the Hellmann-Feynman forces on atoms were smaller than 0.01 eV/Å.

Ab initio molecular dynamics (AIMD) simulations are used to confirm the thermal stability of the graphene/Ga₂SSe heterostructure. AIMD simulations are performed through Nosé thermostat algorithm at a temperature of 300 K for a total of 4 ps with a time step of 1 fs.

The optical absorption of materials can be calculated as follows:

$$\alpha(\omega) = \frac{\sqrt{2}\omega}{c} \left[\sqrt{\varepsilon_1^2(\omega) + \varepsilon_2^2(\omega)} - \varepsilon_1(\omega) \right]^{1/2}. \quad (1)$$

Here, $\varepsilon_i(\omega)$ ($i = 1, 2$) represent the real and imaginary parts of the dielectric functions, respectively. The real part can be obtained from the Kramers-Kronig equation, which is

$$\varepsilon_1(\omega) = 1 + \frac{2}{\pi} P \int_0^\infty \frac{\varepsilon_2(\omega')\omega'}{\omega'^2 - \omega^2 + i\eta} d\omega' \quad (2)$$

III. RESULTS AND DISCUSSION

We first examine all the structural characteristics of single-layer graphene and Janus Ga₂SSe, as displayed in Fig. 1. Graphene has a zero band gap, illustrating a semimetallic character with a Dirac cone at the K point. Unlike graphene, the Janus Ga₂SSe monolayer has a layered atomic structure, as shown in Fig. 1(d). Each Ga₂SSe unit cell consists of four atoms, including two Ga atoms and two chalcogen S and Se atoms in opposite directions. Due to the difference in

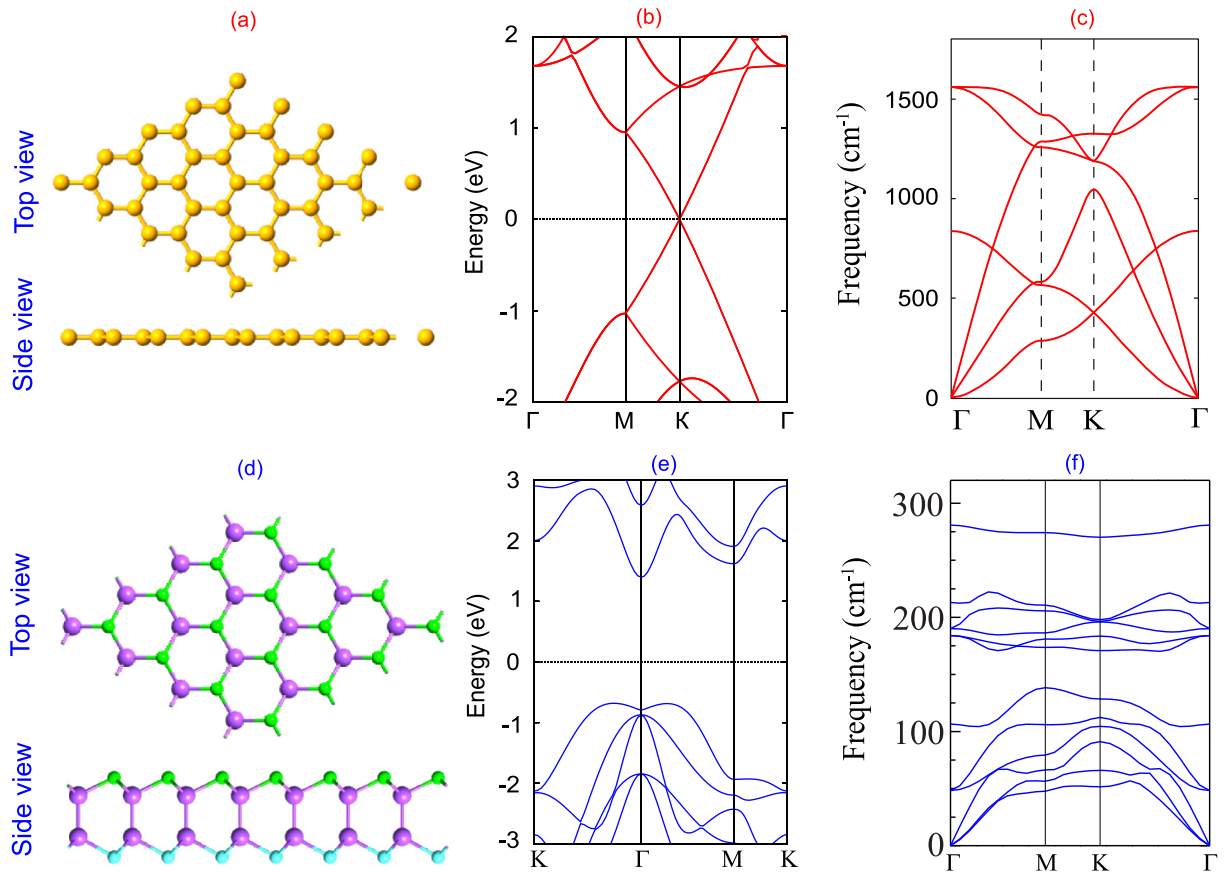


FIG. 1. (a) and (d) Atomic structure, (b) and (e) band structures, and (c) and (f) phonon dispersion curves of perfect graphene and the Janus Ga_2SSe monolayer, respectively. Yellow balls stand for the carbon atoms in graphene, while violet, green, and cyan balls represent the gallium, sulfur, and selenium atoms in Janus Ga_2SSe , respectively.

electronegativity of S and Se atoms, this may result in out-of-plane symmetry breaking. The lattice parameter of the Janus Ga_2SSe monolayer is calculated to be $a = b = 3.72 \text{ \AA}$, which is very consistent with previous reports [67]. Furthermore, Janus Ga_2SSe is an indirect semiconductor. The calculated band gap of Janus Ga_2SSe is 2.04 eV, which also gives good agreement with the value reported by Guo and coworkers [67]. The phonon spectrum of Janus Ga_2SSe in Fig. 1(f) confirms it is dynamically stable at the equilibrium state with no negative phonon frequencies.

The graphene/ Ga_2SSe VHTs are constructed by placing graphene on top of Janus Ga_2SSe . Due to different kinds of chalcogen atoms on opposite sides of Janus Ga_2SSe , this results in the formation of two stacking patterns of graphene/ SGa_2Se and graphene/ SeGa_2S VHTs. Moreover, due to the large difference in lattice parameters of graphene and Janus Ga_2SSe in their unit cells, in order to construct the graphene/ Ga_2SSe VHT, we use a supercell, consisting of a (3×3) graphene supercell and a (2×2) supercell of Janus Ga_2SSe . In addition, when a graphene layer is adsorbed on Janus Ga_2SSe , it tends to form two different stacking configurations of graphene/ Ga_2SSe VHTs; there are top and hollow sites, as shown in Fig. 2. Therefore, we consider four different stacking patterns of graphene/ Ga_2SSe VHTs, namely, H1, H2, T1, and T2, as depicted in Fig. 2. The thermal stability of all these stacking patterns is checked by performing AIMD simulations. These results are displayed in

Fig. 3. It is obvious that there is no distortion in structure in any of the heterostructures after heating them for 4 ps. Also, the change in total energy at 0 ps and after 4 ps is very small, indicating that all these patterns are thermally stable at a room temperature of 300 K, making them feasible, and they can thus be obtained easily in future experiments.

To check the structural stability of these patterns, we further calculate the binding energy, which can be obtained as follows:

$$E_b = \frac{E_H - E_G - E_J}{A}. \quad (3)$$

Here, E_H , E_G , and E_J , respectively, represent the total energies of combined graphene/ Ga_2SSe VHT, isolated (3×3) graphene, and (2×2) Janus Ga_2SSe layers. A stands for the surface area of the considered supercell. The interlayer spacing and binding energy of the graphene/ Ga_2SSe VHT for different stacking patterns are listed in Table I. We find that the interlayer spacings are in the range from 3.35 to 3.42 \AA . It should be noted that these values of interlayer spacing are comparable with other typical graphene-based van der Waals (vdW) heterostructures [60], confirming that the weak vdW interactions bond between the graphene and the Janus Ga_2SSe layers. Furthermore, all stacking patterns of graphene/ Ga_2SSe VHTs imply the negative value of binding energies, exhibiting that they are energetically stable. Stacking pattern H2 has the lowest binding energy of all the

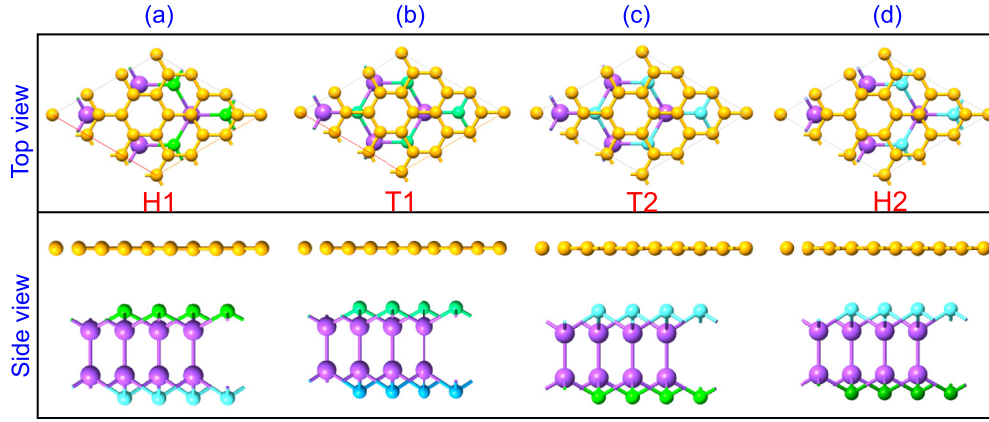


FIG. 2. Relaxed geometric structures of graphene/ Ga_2SSe heterostructures for different stacking patterns: (a) H1, (b) T1, (c) T2, and (d) H2.

configurations, demonstrating that the H2 pattern is the most energetically stable pattern.

The projected band structures of graphene/ Ga_2SSe VHTs for different patterns are depicted in Fig. 4 along with those of the constituent monolayers. The band structures of isolated (3×3) graphene and (2×2) Ga_2SSe monolayers are illustrated in Figs. 4(c) and 4(d), respectively. Owing to the band-folding effect, the linear dispersion relation of graphene is inverted from the K point in perfect graphene into the Γ point in the (3×3) graphene supercell. On the other hand, the Janus Ga_2SSe supercell preserves its semiconducting nature with an indirect band gap of 2.08 eV, which is larger than that of an isolated Ga_2SSe primitive unit cell. The highest (lowest) valence (conduction) band states are positioned in the Γ - K (Γ) point. The valence band (VB) of Janus Ga_2SSe is closer to the Fermi level than the conduction band (CB), demonstrating that Janus Ga_2SSe is a p -type semiconductor. We find that compared to the band structures of both graphene and Ga_2SSe monolayers, the band structures of all stacking patterns of graphene/ Ga_2SSe VHTs are the combinations of those of the constituent monolayers. The Dirac cone of graphene is well

preserved at the Γ point, whereas the semiconducting nature is maintained in Janus Ga_2SSe . This indicates that the electronic properties of both graphene and Ga_2SSe monolayers are well preserved. The nature of such preservation is due to the weak vdW interactions between two constituent monolayers, which keep the heterostructure feasible but are not enough to modify the electronic properties.

More interestingly, when the contact between graphene and Janus Ga_2SSe is formed, a small band gap of about 13–17 meV opens in the graphene layer, depending on the stacking patterns. These values are listed in Table I. The opened band gap in graphene plays an important role in the design of graphene-based high-speed electronic devices. In order to understand the nature of such an opened band gap, we further provide the Hamiltonian of two graphene sublattices as follows:

$$H = \begin{bmatrix} \Delta & \hbar v_F(k_x - ik_y) \\ \hbar v_F(k_x + ik_y) & -\Delta \end{bmatrix},$$

where k is the momentum and v_F is the Fermi velocity. This operator acts on spinors $\psi = \begin{pmatrix} \phi_A \\ \phi_B \end{pmatrix}$, where ϕ_A and ϕ_B are the amplitudes of the wave functions on sublattices A and B, respectively, and Δ is the on-site energies of the A and B sublattices. The dispersion relation near the Fermi level can be approximated as $E(k) = \pm\sqrt{\Delta^2 + (\hbar v_F k)^2}$, the plus (minus) sign corresponds to the conduction (valence) band. For free-standing graphene, the on-site energies of the two sublattices are identical ($\Delta = 0$), resulting in a zero electronic band gap and a linear dispersion relation near the Dirac point. For graphene/ Ga_2SSe heterostructures, the opened band gap is

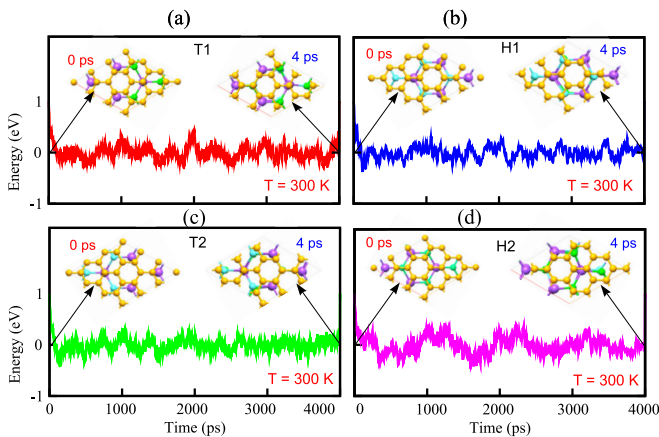


FIG. 3. The AIMD simulation of the change in the total energy as a function of time step at room temperature (300 K) of the graphene/ Ga_2SSe VHT for different patterns: (a) T1, (b) H1, (c) H1, and (d) T2. The insets represent snapshots of atomic structures of the VHT before and after heating for 4 ps.

TABLE I. Calculated interlayer spacing D , binding energy E_b , the opened graphene band gap E_g , and Schottky barrier heights (Φ_n , Φ_p) of the graphene/ Ga_2SSe VHT for different stacking patterns.

	D (Å)	E_b (meV/Å ²)	E_g (meV)	Φ_n (eV)	Φ_p (eV)
T1	3.36	-43.31	13	0.47	1.59
H1	3.42	-50.32	15	0.76	1.33
H2	3.40	-51.35	17	0.76	1.33
T2	3.35	-42.83	14	0.46	1.60

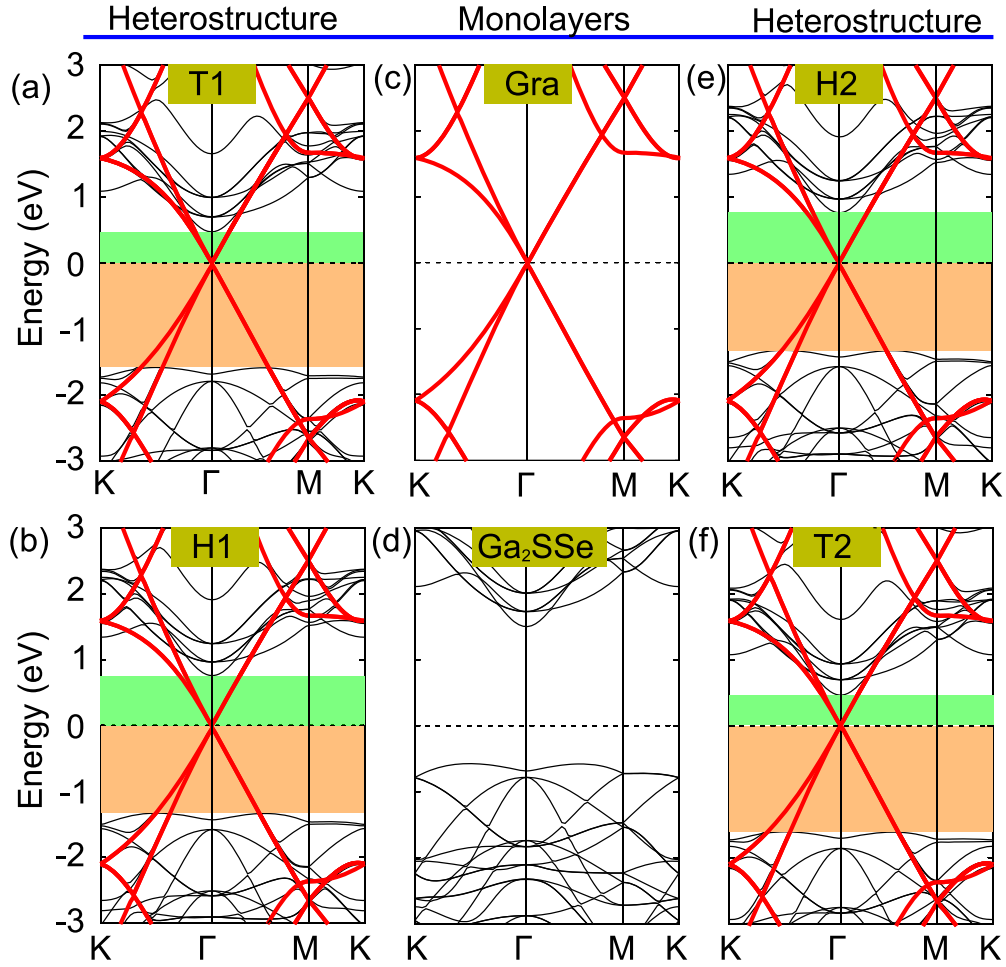


FIG. 4. Projected band structures of graphene/ Ga_2SSe heterostructures for different stacking patterns and their corresponding graphene and Ga_2SSe supercells. Red lines represent the contributions of the graphene layer, while black solid lines represent the contributions of the Janus Ga_2SSe layer.

calculated to be $E_g = 2\Delta$, and a parabolic dispersion relation near the Dirac point is $E(k) \approx \pm(\Delta + \hbar^2 v_F^2 k^2 / 2\Delta)$.

Furthermore, for the use of graphene/ Ga_2SSe VHTs in practical applications, they should have high carrier mobility. It is obvious that the carrier mobility of materials is inversely proportional to the effective mass through the following relation: $\mu = e\tau/m^*$. Thus, to evaluate the carrier mobility of such VHTs, we calculate their effective masses as follows:

$$\frac{1}{m^*} = \frac{1}{\hbar} \frac{\partial^2 E(k)}{\partial k^2}. \quad (4)$$

Here, \hbar and k represent the Planck constant and the wave vector, respectively. From Eq. (4), it can be seen that the effective mass of electrons and of holes can be obtained from the parabolic fitting of the CB and VB of such a heterostructure. Our effective mass for an electron (hole) of the most energetically stacking pattern, H2, of the graphene/ Ga_2SSe VHT at Dirac Γ point is calculated to be $1.56 \times 10^{-3} m_0$ ($2.64 \times 10^{-3} m_0$). The value of the effective mass is quite small, indicating that graphene/ Ga_2SSe VHTs exhibit high carrier mobility. Thus, graphene/ Ga_2SSe VHTs can be considered a potential candidate for future high-speed nanoelectronic applications.

Interestingly, graphene/ Ga_2SSe represents a metal/semiconductor heterojunction, which is characterized by the formation of contact types, including Schottky and Ohmic contacts. We find from Fig. 4 that the graphene/ Ga_2SSe VHT possesses a Schottky contact because its Fermi level lies between the VB and CB of the semiconducting Ga_2SSe layer. It should be noted that the interfacial characteristics and contact types, forming at the graphene/ Ga_2SSe interface, determine its use for practical applications. The formed Schottky contact in graphene/ Ga_2SSe VHT demonstrates that it is suitable for Schottky devices and Schottky diodes. The Schottky barriers are determined following the Schottky-Mott rule [68] as follows: $\Phi_n = E_{CB} - E_F$ and $\Phi_p = E_F - E_{VB}$. As depicted in Fig. 5, the p -type semiconductor in the freestanding Janus Ga_2SSe layer is converted to n type after the formation of the graphene/ Ga_2SSe contact. In addition, the band gap of semiconducting Ga_2SSe also increases to 2.09 eV after contact, which becomes 0.01 eV larger than that of the freestanding form. Our calculations of the Schottky barriers Φ_n and Φ_p are listed in Table I. We find that Φ_n of all stacking patterns of graphene/ Ga_2SSe VHTs is smaller than Φ_p , suggesting that they form a n -type Schottky contact (n -SC type).

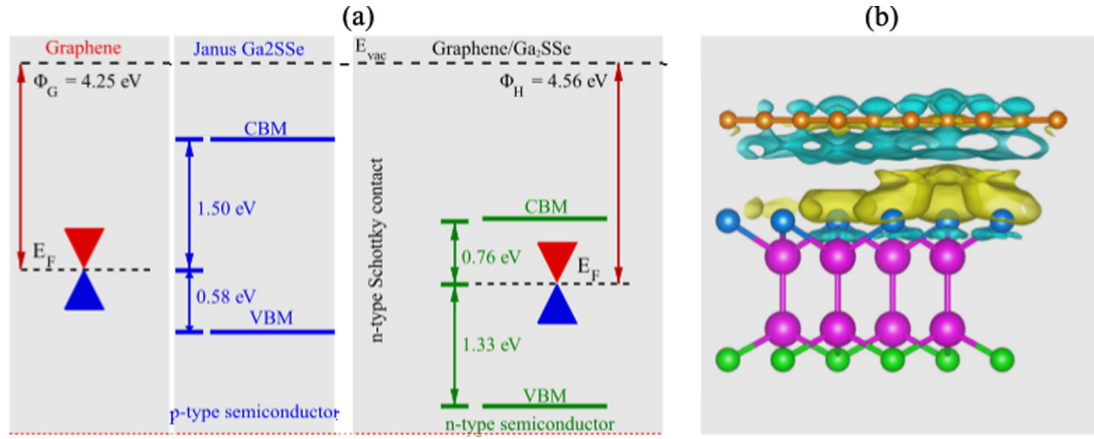


FIG. 5. (a) Band alignment of graphene and Janus Ga₂SSe monolayers before and after contact. (b) Charge density difference of the graphene/Ga₂SSe VHT. Yellow and cyan regions represent charge accumulation and depletion, respectively.

In Fig. 5(b), we provide the charge density difference of the graphene/Ga₂SSe VHT for its most energetically stable pattern to visualize the charge redistribution at the interface. It should be noted that the difference in charge densities is visualized by

$$\Delta\rho(r) = \rho_H(r) - \sum \rho_M(r), \quad (5)$$

where $\rho_H(r)$ and $\rho_M(r)$ represent the charge density of the heterostructure and isolated monolayers, respectively. One can observe from Fig. 5(b) that the charge depletion region is around the graphene layer, indicating that graphene loses electrons and becomes a hole-rich region. While the charge accumulation area is around the selenium surface of Janus Ga₂SSe, it becomes an electron-rich surface. It also suggests that the electrons are transferred from the graphene to the Ga₂SSe layer in their combined graphene/Ga₂SSe VHT.

Actually, for use in practical applications of photocatalytic nanodevices, such a Ga₂SSe VHT should absorb as much light in the visible and ultraviolet (UV) regions as possible. Therefore, we further consider the optical properties of graphene/Ga₂SSe VHT by calculating the real and imaginary parts of the dielectric functions and the optical absorption coefficient. These performances of the graphene/Ga₂SSe VHT

as well as those of single-layer monolayers are displayed in Fig. 6. The real part $\varepsilon_1(\omega)$ is associated with the stored energy within the medium, and the imaginary part $\varepsilon_2(\omega)$ is associated with the dissipation of energy within that medium [69]. The static dielectric constant $\varepsilon_0(\omega)$ is the most important part of the real part. As presented in Fig. 6(a), the calculated values of $\varepsilon_0(\omega)$ for graphene and Ga₂SSe monolayer are 1.15 and 2.55 eV, respectively. The calculated values are close to those of previous theoretical calculations [70,71]. It can also be noticed that $\varepsilon_0(\omega)$ is increased to reach a value of 2.75 for the graphene/Ga₂SSe heterostructure. The imaginary part $\varepsilon_2(\omega)$ of the dielectric function is presented in Fig. 6(b). The $\varepsilon_2(\omega)$ spectrum of the Ga₂SSe monolayer exhibits an intense absorption peak near the visible region, suggesting the visible-light absorption capability of the studied monolayer. The $\varepsilon_2(\omega)$ spectrum of graphene is very weak compared to that of the Ga₂SSe monolayer. One may also notice that the $\varepsilon_2(\omega)$ spectrum of the graphene/Ga₂SSe VHT is slightly redshifted compared to that of the individual monolayers. Furthermore, the absorption intensity of the $\varepsilon_2(\omega)$ spectrum for the graphene/Ga₂SSe heterostructure overlaps with that of Ga₂SSe but is higher than that of graphene. This indicates the good absorption capability of the constructed heterostructure. Moreover, the formation of the heterostructure

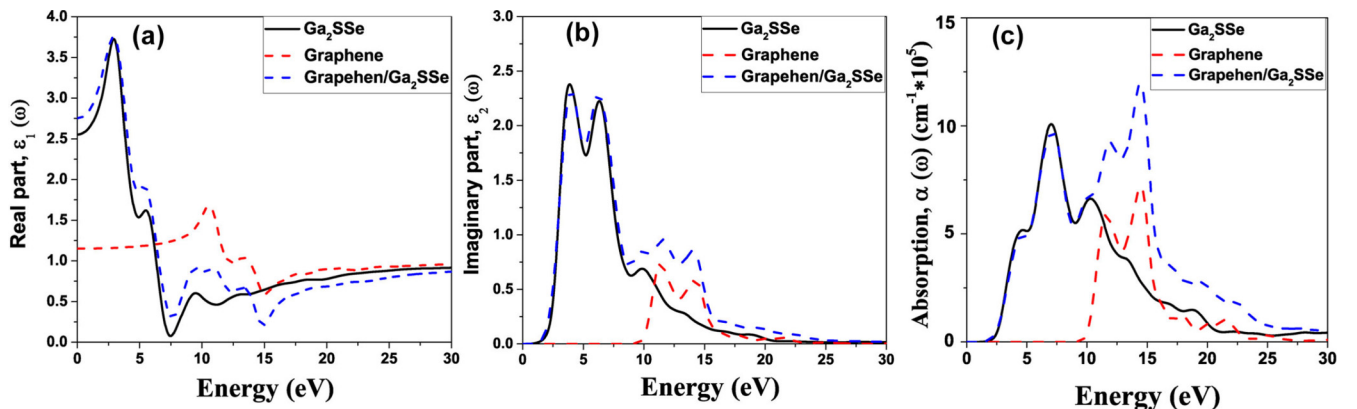


FIG. 6. (a) Real and (b) imaginary parts of dielectric functions and (c) optical absorption of the graphene/Ga₂SSe VHT and the individual monolayers along the z axis.

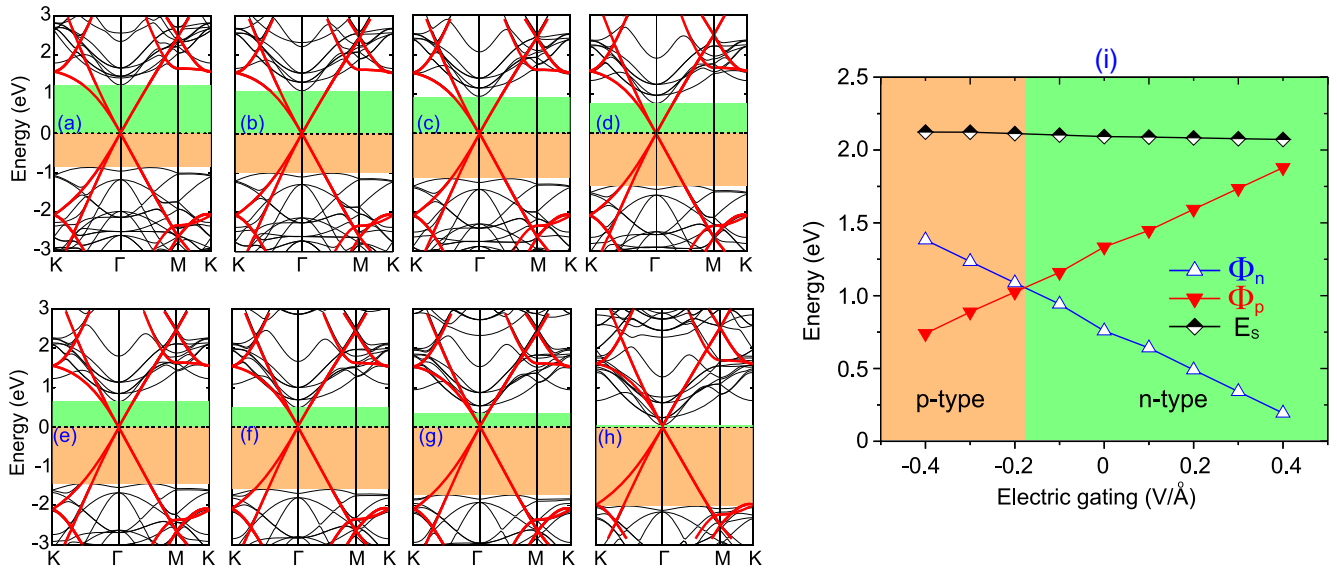


FIG. 7. Projected band structures of the graphene/Ga₂SSe heterostructure under negative electric gating of (a) -0.3 V/Å, (b) -0.2 V/Å, (c) -0.1 V/Å, and (d) 0 V/Å and positive electric gating of (e) 0 V/Å, (f) $+0.1$ V/Å, (g) $+0.2$ V/Å, and (h) $+0.3$ V/Å. Red lines represent the contributions of the graphene supercell. (i) The variations of SBH as a function of electric gating.

also leads to an increase in the optical absorption in the visible and UV regions compared to the constituent monolayers [see Fig. 6(c)]. A similar trend has been predicted for other heterostructures [72,73]. It can be concluded that the designed heterostructure maintains the intrinsic optical properties of the individual graphene and Ga₂SSe monolayer and also displays some distinguished optical features, such as enhanced absorption intensity, a peculiar dielectric function, and a wide range of photoresponse, which is promising for applications in optical transmission and photoelectric devices.

From a device viewpoint, the contact types and Schottky barriers of the graphene/Ga₂SSe VHT are one of the most important challenges that strongly affect the device's performance and possibilities. Thus, in order to evaluate the effectiveness of the graphene/Ga₂SSe VHT for the design of high-performance nanodevices, we further consider whether the contact types and Schottky barriers of such a VHT could be adjusted by electric gating and interlayer coupling. The projected band structures and the changes in the contact types and Schottky barrier height (SBH) of graphene/Ga₂SSe VHT under electric gating are depicted in Fig. 7. Obviously, the positions of the VB and CB relative to the Fermi level of the semiconducting Ga₂SSe part are shifted under electric gating, as depicted in Figs. 7(a)–7(h). Such a thing leads to changes in the SBH of the graphene/Ga₂SSe VHT, as shown in Fig. 7(i). The electric gating, pointing from the Ga₂SSe to the graphene layer, is assigned as the positive direction. Under negative electric gating, we find that Φ_p decreases linearly with decreasing negative gating, whereas Φ_n increases accordingly. We can observe that under negative gating of -0.2 V/Å, Φ_p decreases and becomes smaller than Φ_n, suggesting the possibility to switch from *n*-SC to *p*-SC type. The physical mechanism of such a possibility to switch can be explained by a shift in the Fermi level. The negative gating shifts the Fermi level towards the lower binding energies, i.e., towards the VB of the semiconducting Ga₂SSe part. It indicates that

the Fermi level of such a VHT is closer to the VB than to the CB, leading to such a possibility to switch.

On the other hand, when the positive electric gating is introduced, Φ_p increases linearly, while Φ_n decreases accordingly. For positive gating, Φ_n decreases and is smaller than Φ_p, implying that the graphene/Ga₂SSe VHT remains to be of the *n*-SC type, as depicted in Fig. 7(i). Interestingly, due to a linear decrease in Φ_n with increasing positive gating, our results predict that Φ_n can decrease to zero under a positive gating of $+0.37$ V/Å. The zero and negative values of SBH demonstrate that the graphene/Ga₂SSe VHT is characterized by an Ohmic contact, suggesting that such a VHT is quite acceptable for semiconductor applications in which the graphene layer acts as a transparent electrode and the semiconducting Ga₂SSe layer acts as a channel. The nature of the variation of Φ_p and Φ_n under positive electric gating is due to the shift of the Fermi level. When the positive electric gating is introduced, the Fermi level is shifted towards the CB of the semiconducting part. It indicates the Fermi level is getting closer to the CB of the Ga₂SSe part, implying that the graphene/Ga₂SSe VHT remains to be of the *n*-SC type. Under an electric gating of $+0.37$ V/Å, the Fermi level continuously moves upwards and crosses the CB of the Ga₂SSe layer, resulting in the transition from an *n*-SC to Ohmic type of contact. From all the above-mentioned results, we find that electric gating can tune the SBH and contact types of the graphene/Ga₂SSe VHT from *n*-SC type to *p*-SC and to Ohmic type.

The projected band structures of the graphene/Ga₂SSe heterostructure under different interlayer spacings and the variation of the SBH as a function of interlayer spacings are depicted in Fig. 8. Obviously, the decrease in interlayer spacing from the equilibrium value leads to a narrowed Φ_p and a heightened Φ_n. One can observe from Fig. 8(g) that when the interlayer spacing is smaller than 3.0 Å, Φ_p becomes narrower than Φ_n, resulting in the possibility of switching from *n*-SC to *p*-SC type in the graphene/Ga₂SSe VHT. Meanwhile,

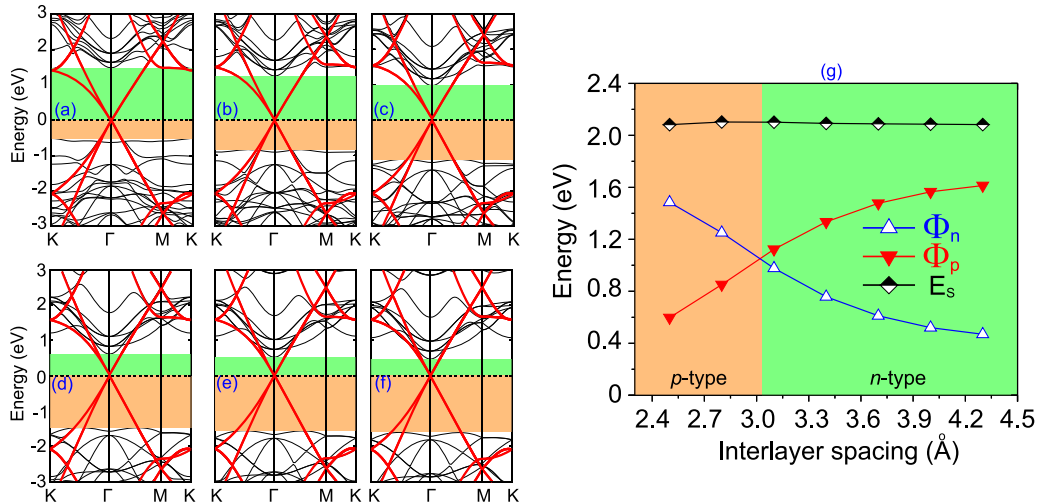


FIG. 8. Projected band structures of the graphene/ Ga_2SSe heterostructure under different interlayer spacings of (a) 2.5 Å, (b) 2.8 Å, (c) 3.1 Å, (d) 3.7 Å, (e) 4.0 Å, and (f) 4.3 Å. Red lines represent the contributions of the graphene supercell. (g) The changes in the SBH of the graphene/ Ga_2SSe heterostructure as a function of interlayer spacing.

the opposite change in Φ_p and Φ_n by increasing interlayer spacing is observed. The n -SC type is still maintained in the graphene/ Ga_2SSe VHT. The physical mechanism of the Φ_p and Φ_n variations can be explained by further analyzing the projected band structures of the graphene/ Ga_2SSe VHT under different interlayer spacings. As interlayer spacing decreases, the Dirac cone of graphene shifts towards the VB of the semiconducting part. However, by increasing the interlayer spacing away from the equilibrium value, the graphene Dirac cone moves upwards to higher binding energy, i.e., to the CB of the Ga_2SSe part. When the interlayer spacing is smaller than 3.0 Å, the graphene Dirac cone is closer to the VB than the CB of the semiconducting Ga_2SSe layer, confirming that the graphene/ Ga_2SSe VHT is characterized by the p -SC type. From the results discussed above, we can conclude that a change in the interlayer spacing can induce a change from n -SC to p -SC type, making the graphene/ Ga_2SSe VHT a potential candidate for future Schottky nanodevices. It is clear that in the view of device application, the interlayer spacing is an effective way to improve the performance of electronic devices. Therefore, the engineering of interlayer spacing can work on not only efficiently controlling the interface contact type but also the SBHs of the graphene/ Ga_2SSe VHT, which is important for improving the performances of the controllable nanoelectronic and optoelectronic devices.

IV. CONCLUSION

In summary, we have used first-principles simulations to study the electronic, interfacial properties and optical per-

formance of the graphene/ Ga_2SSe heterostructures. Different favorable stacking patterns of graphene/ Ga_2SSe heterostructures were also constructed and examined. Our results show that all the stacking patterns of graphene/ Ga_2SSe heterostructures are energetically and thermally stable at room temperature, such that they can be fabricated in experiments. In the graphene/ Ga_2SSe heterostructures, the Dirac cone of graphene is well preserved at the Γ point owing to the weak vdW interactions, which keep the heterostructures feasible. After the formation of a graphene/ Ga_2SSe contact, a small band gap of about 13–17 meV opens in graphene due to symmetry breaking. The graphene/ Ga_2SSe heterostructures also shows high carrier mobility, making them potential candidates for future high-speed nanoelectronic applications. Furthermore, the graphene/ Ga_2SSe heterostructures form an n -type Schottky contact. The transformation from the n -type to p -type Schottky contact or to Ohmic contact can be forced by electric gating or by varying the interlayer coupling. Our findings could provide physical guidance for designing controllable Schottky nanodevices with high electronic and optical performances.

ACKNOWLEDGMENT

This research is funded by Vietnam National Foundation for Science and Technology Development (NAFOSTED) under Grant No. 103.01-2019.05.

The authors declare that there are no conflicts of interest regarding the publication of this paper.

- [1] K. S. Novoselov, A. K. Geim, S. V. Morozov, D. Jiang, Y. Zhang, S. V. Dubonos, I. V. Grigorieva, and A. A. Firsov, *Science* **306**, 666 (2004).
 [2] X. Du, I. Skachko, A. Barker, and E. Y. Andrei, *Nat. Nanotechnol.* **3**, 491 (2008).

- [3] K. I. Bolotin, F. Ghahari, M. D. Shulman, H. L. Stormer, and P. Kim, *Nature (London)* **462**, 196 (2009).
 [4] F. Schwierz, *Nat. Nanotechnol.* **5**, 487 (2010).
 [5] J. K. Wassei and R. B. Kaner, *Mater. Today* **13**, 52 (2010).

- [6] Z. Ma, B. Wang, L. Ou, Y. Zhang, X. Zhang, and Z. Zhou, *Nanotechnology* **27**, 415203 (2016).
- [7] K. F. Mak, C. Lee, J. Hone, J. Shan, and T. F. Heinz, *Phys. Rev. Lett.* **105**, 136805 (2010).
- [8] J.-H. Lin, H. Zhang, X.-L. Cheng, and Y. Miyamoto, *Phys. Rev. B* **96**, 035438 (2017).
- [9] A. Carvalho, M. Wang, X. Zhu, A. S. Rodin, H. Su, and A. H. C. Neto, *Nat. Rev. Mater.* **1**, 1 (2016).
- [10] H. Wang, C. Zhang, W. Chan, S. Tiwari, and F. Rana, *Nat. Commun.* **6**, 1 (2015).
- [11] V. Podzorov, M. Gershenson, C. Kloc, R. Zeis, and E. Bucher, *Appl. Phys. Lett.* **84**, 3301 (2004).
- [12] S. Das, M. Demarteau, and A. Roelofs, *ACS Nano* **8**, 11730 (2014).
- [13] S. Manzeli, D. Ovchinnikov, D. Pasquier, O. V. Yazyev, and A. Kis, *Nat. Rev. Mater.* **2**, 17033 (2017).
- [14] C. Mu, J. Xiang, and Z. Liu, *J. Mater. Res.* **32**, 4115 (2017).
- [15] N. Zibouche, A. Kuc, J. Musfeldt, and T. Heine, *Ann. Phys. (Berlin, Ger.)* **526**, 395 (2014).
- [16] L. C. Gomes and A. Carvalho, *Phys. Rev. B* **92**, 085406 (2015).
- [17] Z. Tian, C. Guo, M. Zhao, R. Li, and J. Xue, *ACS Nano* **11**, 2219 (2017).
- [18] H. Liu, A. T. Neal, Z. Zhu, Z. Luo, X. Xu, D. Tománek, and P. D. Ye, *ACS Nano* **8**, 4033 (2014).
- [19] S. Yang, Y. Gong, J. Zhang, L. Zhan, L. Ma, Z. Fang, R. Vajtai, X. Wang, and P. M. Ajayan, *Adv. Mater.* **25**, 2452 (2013).
- [20] Q. Liang, Z. Li, Z.-H. Huang, F. Kang, and Q.-H. Yang, *Adv. Funct. Mater.* **25**, 6885 (2015).
- [21] C. R. Dean, A. F. Young, I. Meric, C. Lee, L. Wang, S. Sorgenfrei, K. Watanabe, T. Taniguchi, P. Kim, K. L. Shepard *et al.*, *Nat. Nanotechnol.* **5**, 722 (2010).
- [22] B. Radisavljevic, A. Radenovic, J. Brivio, V. Giacometti, and A. Kis, *Nat. Nanotechnol.* **6**, 147 (2011).
- [23] D. Pierucci, H. Henck, C. H. Naylor, H. Sediri, E. Lhuillier, A. Balan, J. E. Rault, Y. J. Dappe, F. Bertran, P. Le Fèvre *et al.*, *Sci. Rep.* **6**, 26656 (2016).
- [24] D. Pierucci, H. Henck, J. Avila, A. Balan, C. H. Naylor, G. Patriarche, Y. J. Dappe, M. G. Silly, F. Sirotti, A. C. Johnson *et al.*, *Nano Lett.* **16**, 4054 (2016).
- [25] Q. Peng, Z. Wang, B. Sa, B. Wu, and Z. Sun, *Sci. Rep.* **6**, 31994 (2016).
- [26] N. Huo, J. Kang, Z. Wei, S.-S. Li, J. Li, and S.-H. Wei, *Adv. Funct. Mater.* **24**, 7025 (2014).
- [27] F. Dong, T. Xiong, Y. Sun, Y. Zhang, and Y. Zhou, *Chem. Commun.* **51**, 8249 (2015).
- [28] H. U. Din, M. Idrees, A. Albar, M. Shafiq, I. Ahmad, C. V. Nguyen, and B. Amin, *Phys. Rev. B* **100**, 165425 (2019).
- [29] X. Zhou, N. Zhou, C. Li, H. Song, Q. Zhang, X. Hu, L. Gan, H. Li, J. Lü, J. Luo *et al.*, *2D Mater.* **4**, 025048 (2017).
- [30] T. Georgiou, R. Jalil, B. D. Belle, L. Britnell, R. V. Gorbachev, S. V. Morozov, Y.-J. Kim, A. Gholinia, S. J. Haigh, O. Makarovsky *et al.*, *Nat. Nanotechnol.* **8**, 100 (2013).
- [31] F. Yan, Z. Wei, X. Wei, Q. Lv, W. Zhu, and K. Wang, *Small Methods* **2**, 1700349 (2018).
- [32] H. Coy Diaz, J. Avila, C. Chen, R. Addou, M. C. Asensio, and M. Batzill, *Nano Lett.* **15**, 1135 (2015).
- [33] S. Singh, C. Espejo, and A. H. Romero, *Phys. Rev. B* **98**, 155309 (2018).
- [34] S. Bertolazzi, D. Krasnozhan, and A. Kis, *ACS Nano* **7**, 3246 (2013).
- [35] Y. Li, W. Wu, and F. Ma, *J. Mater. Chem. A* **7**, 611 (2019).
- [36] J. E. Padilha, A. Fazzio, and A. J. R. da Silva, *Phys. Rev. Lett.* **114**, 066803 (2015).
- [37] R. Li, W. Sun, C. Zhan, P. R. C. Kent, and D.-e. Jiang, *Phys. Rev. B* **99**, 085429 (2019).
- [38] S. Zhou, X. Yang, W. Pei, N. Liu, and J. Zhao, *Nanoscale* **10**, 10876 (2018).
- [39] I. Demiroglu, F. M. Peeters, O. Gülseren, D. Çakır, and C. Sevik, *J. Phys. Chem. Lett.* **10**, 727 (2019).
- [40] D. S. Koda, F. Bechstedt, M. Marques, and L. K. Teles, *Phys. Rev. B* **97**, 165402 (2018).
- [41] X. Gao, Y. Shen, Y. Ma, S. Wu, and Z. Zhou, *Carbon* **146**, 337 (2019).
- [42] S. Wang, J.-P. Chou, C. Ren, H. Tian, J. Yu, C. Sun, Y. Xu, and M. Sun, *Sci. Rep.* **9**, 1 (2019).
- [43] T. V. Vu, T. P. Dao, M. Idrees, H. V. Phuc, N. N. Hieu, N. T. Binh, H. B. Dinh, B. Amin, and C. V. Nguyen, *Phys. Chem. Chem. Phys.* **22**, 7952 (2020).
- [44] Z. Ben Aziza, H. Henck, D. Pierucci, M. G. Silly, E. Lhuillier, G. Patriarche, F. Sirotti, M. Eddrief, and A. Ouerghi, *ACS Nano* **10**, 9679 (2016).
- [45] Z. Ben Aziza, D. Pierucci, H. Henck, M. G. Silly, C. David, M. Yoon, F. Sirotti, K. Xiao, M. Eddrief, J. C. Girard, and A. Ouerghi, *Phys. Rev. B* **96**, 035407 (2017).
- [46] H. V. Phuc, V. V. Ilysov, N. N. Hieu, B. Amin, and C. V. Nguyen, *J. Alloys Compd.* **750**, 765 (2018).
- [47] K. D. Pham, N. N. Hieu, H. V. Phuc, I. Fedorov, C. Duque, B. Amin, and C. V. Nguyen, *Appl. Phys. Lett.* **113**, 171605 (2018).
- [48] F. Ning, D. Wang, Y.-X. Feng, L.-M. Tang, Y. Zhang, and K.-Q. Chen, *J. Mater. Chem. C* **5**, 9429 (2017).
- [49] A.-Y. Lu, H. Zhu, J. Xiao, C.-P. Chuu, Y. Han, M.-H. Chiu, C.-C. Cheng, C.-W. Yang, K.-H. Wei, Y. Yang *et al.*, *Nat. Nanotechnol.* **12**, 744 (2017).
- [50] J. Zhang, S. Jia, I. Kholmanov, L. Dong, D. Er, W. Chen, H. Guo, Z. Jin, V. B. Shenoy, L. Shi *et al.*, *ACS Nano* **11**, 8192 (2017).
- [51] T. Hu, F. Jia, G. Zhao, J. Wu, A. Stroppa, and W. Ren, *Phys. Rev. B* **97**, 235404 (2018).
- [52] M. Yagmurcukardes, C. Sevik, and F. M. Peeters, *Phys. Rev. B* **100**, 045415 (2019).
- [53] A. Huang, W. Shi, and Z. Wang, *J. Phys. Chem. C* **123**, 11388 (2019).
- [54] M. Yagmurcukardes and F. M. Peeters, *Phys. Rev. B* **101**, 155205 (2020).
- [55] Y.-D. Guo, H.-B. Zhang, H.-L. Zeng, H.-X. Da, X.-H. Yan, W.-Y. Liu, and X.-Y. Mou, *Phys. Chem. Chem. Phys.* **20**, 21113 (2018).
- [56] K. D. Pham, N. N. Hieu, H. V. Phuc, B. D. Hoi, V. V. Ilysov, B. Amin, and C. V. Nguyen, *Computat. Mater. Sci.* **153**, 438 (2018).
- [57] L. S. Cavalcante, M. N. Gjerding, A. Chaves, and K. S. Thygesen, *J. Phys. Chem. C* **123**, 16373 (2019).
- [58] T. V. Vu, N. V. Hieu, H. V. Phuc, N. N. Hieu, H. Bui, M. Idrees, B. Amin, and C. V. Nguyen, *Appl. Surf. Sci.* **507**, 145036 (2020).
- [59] S. Deng, L. Li, and P. Rees, *ACS Appl. Nano Mater.* **2**, 3977 (2019).

- [60] L. Cao, Y. S. Ang, Q. Wu, and L. Ang, *Appl. Phys. Lett.* **115**, 241601 (2019).
- [61] S. K. Chong, F. Long, G. Wang, Y.-C. Lin, S. Bhandari, R. Shahbazian-Yassar, K. Suenaga, R. Pandey, and Y. K. Yap, *ACS Appl. Nano Mater.* **1**, 3293 (2018).
- [62] P. Giannozzi, O. Andreussi, T. Brumme, O. Bunau, M. B. Nardelli, M. Calandra, R. Car, C. Cavazzoni, D. Ceresoli, M. Cococcioni, N. Colonna, I. Carnimeo, A. D. Corso, S. de Gironcoli, P. Delugas, R. A. DiStasio, A. Ferretti, A. Floris, G. Fratesi, G. Fugallo, R. Gebauer, U. Gerstmann, F. Giustino, T. Gorni, J. Jia, M. Kawamura, H.-Y. Ko, A. Kokalj, E. Küçükbenli, M. Lazzeri, M. Marsili, N. Marzari, F. Mauri, N. L. Nguyen, H.-V. Nguyen, A. O. de-la Roza, L. Paulatto, S. Poncé, D. Rocca, R. Sabatini, B. Santra, M. Schlipf, A. P. Seitsonen, A. Smogunov, I. Timrov, T. Thonhauser, P. Umari, N. Vast, X. Wu, and S. Baroni, *J. Phys.: Condens. Matter* **29**, 465901 (2017).
- [63] P. Giannozzi, S. Baroni, N. Bonini, M. Calandra, R. Car, C. Cavazzoni, D. Ceresoli, G. L. Chiarotti, M. Cococcioni, I. Dabo, A. D. Corso, S. de Gironcoli, S. Fabris, G. Fratesi, R. Gebauer, U. Gerstmann, C. Gougoussis, A. Kokalj, M. Lazzeri, L. Martin-Samos, N. Marzari, F. Mauri, R. Mazzarello, S. Paolini, A. Pasquarello, L. Paulatto, C. Sbraccia, S. Scandolo, G. Sclauzero, A. P. Seitsonen, A. Smogunov, P. Umari, and R. M. Wentzcovitch, *J. Phys.: Condens. Matter* **21**, 395502 (2009).
- [64] J. P. Perdew, K. Burke, and M. Ernzerhof, *Phys. Rev. Lett.* **77**, 3865 (1996).
- [65] J. P. Perdew, K. Burke, and M. Ernzerhof, *Phys. Rev. Lett.* **80**, 891 (1998).
- [66] P. E. Blöchl, *Phys. Rev. B* **50**, 17953 (1994).
- [67] Y. Guo, S. Zhou, Y. Bai, and J. Zhao, *Appl. Phys. Lett.* **110**, 163102 (2017).
- [68] J. Bardeen, *Phys. Rev.* **71**, 717 (1947).
- [69] A. Bafekry, M. Obeid, C. Nguyen, M. B. Tagani, and M. Ghergherehchi, *J. Mater. Chem. A* **8**, 13248 (2020).
- [70] P. Rani, G. S. Dubey, and V. Jindal, *Phys. E (Amsterdam, Neth.)* **62**, 28 (2014).
- [71] H. R. Jappor, M. M. Obeid, T. V. Vu, D. Hoat, H. D. Bui, N. N. Hieu, S. J. Edrees, Y. Mogulkoc, and R. Khenata, *Superlattices Microstruct.* **130**, 545 (2019).
- [72] C. V. Nguyen, T. P. Dao, T. T. Tho, L. T. Hoa, N. N. Hieu, H. V. Phuc, M. Idrees, B. Amin, and P. Le, *Diamond Relat. Mater.* **106**, 107851 (2020).
- [73] H.-Y. Wu, K. Yang, Y. Si, W.-Q. Huang, W. Hu, and G.-F. Huang, *Phys. Status Solidi RRL* **13**, 1800565 (2019).